Nuclear Engineering and Technology 51 (2019) 987–995

Contents lists available at ScienceDirect

Nuclear Engineering and Technology

journal homepage: www.elsevier.com/locate/net

Original Article

Experimental study on the condensation of sonic steam in the underwater environment

Zhaoming Meng [a, *], Wei Zhang [a, b], Jiazhi Liu [a], Ruihao Yan [a], Geyu Shen [a]

[a] Fundamental Science on Nuclear Safety and Simulation Technology Laboratory, Harbin Engineering University, Harbin, Heilongjiang, 150001, China
[b] School of Nuclear Science and Engineering, Shanghai Jiao Tong University, 800 Dong Chuang Road, Shanghai, 200240, China

ARTICLE INFO

Article history:
Received 15 August 2018
Received in revised form
29 December 2018
Accepted 2 February 2019
Available online 6 February 2019

Keywords:
Direct contact condensation
Sonic jet
Condensation regimes
Condensation heat transfer coefficients

ABSTRACT

Steam jet condensation is of great importance to pressure suppression containment and automatic depressurization system in nuclear power plant. In this paper, the condensation processes of sonic steam jet in a quiescent subcooled pool are recorded and analyzed, more precise understanding are got in direct contact condensation. Experiments are conducted at atmospheric pressure, and the steam is injected into the subcooled water pool through a vertical nozzle with the inner diameter of 10 mm, water temperature in the range of 25–60 °C and mass velocity in the range of 320–1080 kg/m^{2}s. Richardson number is calculated based on the conservation of momentum for single water jet and its values are in the range of 0.16–2.67. There is no thermal stratification observed in the water pool. Four condensation regimes are observed, including condensation oscillation, contraction, expansion-contraction and double expansion-contraction shapes. A condensation regime map is present based on steam mass velocity and water temperature. The dimensionless steam plume length increase with the increase of steam mass velocity and water temperature, and its values are in the range of 1.4–9.0. Condensation heat transfer coefficient decreases with the increase of steam mass velocity and water temperature, and its values are in the range of 1.44–3.65 MW/m^2°C. New more accurate semi-empirical correlations for prediction of the dimensionless steam plume length and condensation heat transfer coefficient are proposed respectively. The discrepancy of predicted plume length is within ± 10% for present experimental results and ± 25% for previous researchers. The discrepancy of predicted condensation heat transfer coefficient is with ± 12%.

1. Introduction

Steam jet condensation in pool is an effective method to rapid pressure relief for high temperature and high pressure water/steam systems. In the advanced light water reactor designs, pressure suppression system for reactor pressure vessel and containment are widely used to ensure the safety of nuclear power plant, such as pressure suppression pool, in-containment refueling water storage tank, air hold tank [1] and bubble condenser [2]. So, the study on the steam jet condensation is really helpful to the pressure suppression system designs.

Involving in two phase flow, with interfacial instability, gas dynamic effects, phase change and entrainment, steam jet condensation process is extremely complex. Many researchers have investigated steam jet condensation in subcooled pool, mainly including condensation regime, liquid phase dependent parameters and two phase interfacial parameters.

Firstly, during the steam jet injection, various characteristics are observed according to different steam mass velocity and water temperature. Condensation regime maps have been given by many researchers [3–8]. Cho et al. [5] presented a condensation regime map based on the experimental observation, which had a wide scope of application, as shown in Fig. 1. At low steam mass velocity, chugging(C) occurs, where water enters into the nozzle periodic and causes high amplitude pressure pulse. At middle steam mass velocity, condensation oscillation (CO) occurs, where water does not enter into the nozzle. At high steam mass velocity, stable condensation (SC) occurs, where steam-water interface has a regular shape. A transient regime (TC) is found between chugging and condensation oscillation. As the water temperature increases, bubbling condensation oscillation (BCO) and interfacial oscillation condensation (IOC) occurs.

Besides, a condensation regime diagram for supersonic and subsonic steam jet condensation was presented by Xu et al. [9].

* Corresponding author.
E-mail address: mengzhaoming@hrbeu.edu.cn (Z. Meng).

https://doi.org/10.1016/j.net.2019.02.003

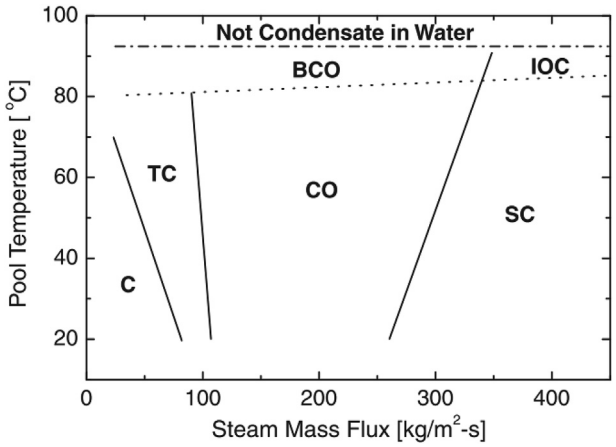

Fig. 1. Condensation regime map by Cho [5].

With different classification, they assert that scaled steam mass flux is irrelevant to the transitional lines in the regime diagram and condensation regime diagram at low ambient pressure can be applied to high pressure.

On top of that, studies of liquid phase dependent parameters generally involve pressure oscillation, temperature distribution and velocity distribution. Pressure oscillation consists of low, middle and high frequency components for stable condensation, due to turbulent vortexes [10], periodical variation of steam plume length [11] and separated steam bubbles oscillation [12,13]. As known, consistent conclusion is obtained that pressure oscillation frequency decreases with the increase of steam mass velocity and water temperature for stable condensation. However, for condensation oscillation regime, there is no consistent conclusion about the effect of steam mass velocity on the pressure oscillation frequency. Fukuda [14] presented steam mass velocity has little effect on oscillation frequency, while Hong et al. [11] presented oscillation frequency decreases with the increase of steam mass velocity. Recently, Yuan et al. [15] thought oscillation frequency increases with the increase of steam mass velocity. Hence, this is still a doubtful point.

For the thermal distribution, Wu et al. [16] and Yang et al. [17] presented axial temperature distribution can represent different condensation regimes and give evidence of the existence of expansion and compression waves. Song et al. [18] presented dimensional analysis using synthetic jet theory and gave critical Richardson number based on experiment results. Hua [19] presented effective heat source and effective momentum source models to simulate thermal stratification and mixing for steam injection through vertical pipe. Song et al. [20] presented there is close relationship between thermal stratification and flow patterns in the pool by using the PIV technique. Choo and Song [21] found turbulent water jet produced by steam jet has a good self-similarity feature, which is very similar to single phase water jet [22].

In addition, studies of two phase interfacial parameters involve steam plume parameters (shapes, length and expansion ratio), condensation heat transfer coefficient and interfacial instability. Conical, ellipsoidal and divergent shapes of steam plume were observed by Chun et al. [5] and Kim et al. [8]. Later, four different steam plume shapes (contraction shape, expansion–contraction shape, double expansion–contraction shape, double expansion–divergent shape) were observed for sonic jet by Wu et al. [16], and another two shapes (contraction–expansion–contraction and contraction–expansion–divergent) were observed in the case of supersonic steam jet [23]. Several correlations to predict the dimensionless length of steam plume were given by many researchers [4,23–27]. Kim et al. [28] analyzed condensation heat transfer coefficient based on interfacial transport model, surface renewal model and shear stress model. Chun et al. [4], Kim et al. [25] and Wu et al. [23] gave several correlations for predicting condensation heat transfer coefficient under the assumption of a constant Stanton number. Khan et al. [29] studied the creation and propagation of Kelvin–Helmholtz instabilities in steam jet condensation by measuring the transient temperature fluctuation. They found that the instabilities were originated at the two phase interface and spread to the axis of nozzle.

According to the above references, almost all the research on the sonic steam jet condensation is in the case of the horizontal direction and a large bias is obvious among different correlations. The objective of present experimental study is to study condensation characteristics of the sonic steam jet in vertical direction, including thermal stratification and mixing, condensation regime, steam plume length and condensation heat transfer coefficient. The effects of steam mass velocity, water temperature on condensation characteristics are discussed. The results would offer basic data for CFD validation and engineering design for pressure suppression system.

2. Experimental apparatus

As presented in Fig. 2 (a), the experimental system mainly consists of a steam supply system, a water pool (500mm × 1000mm × 2000mm) and nozzle. The electric steam generator is used to produce pure saturated steam, and its maximum operating pressure is 1.0 MPa and the maximum steam flow rate is 1 t/h. The steam volume flow rate is measured by a vortex flow meter with the range of 0–300 m^3/h and maximum relative deviation of 0.5%. In order to query steam density based on pressure, a pressure sensor with the range of 0–1 MPa and maximum relative deviation 0.5% is installed in the downstream of flow meter. All the stainless steel steam line is insulated with aluminosilicate fiber covering and preheated 30 min before each experiment.

Water pool is open to the atmosphere with six polymethyl methacrylate glasses equipped for video camera imaging and supplementary lighting (see Fig. 2 (a)). An overflow tube with inner diameter 50 mm is used to avoid water level change due to the change of water temperature and condensation. A tap water tube is used to initial replenishment of water and water temperature control for high steam mass velocity case. As presented in Fig. 2 (b), eight K type thermocouples with accuracy of 0.5 °C are installed inside the water pool to measure the water temperature distribution in vertical direction. Each thermocouple is vertically spaced 200 mm and horizontally 150 mm from the nozzle axis. The stainless-steel nozzle with an inner diameter of 10 mm, an outer diameter of 14 mm and a length of 100 mm is installed in the center of the tank along the vertical direction. All signals expect video images are processed by NI data acquisition system. The experimental conditions are shown in Table 1.

A high-speed video camera together with LED lamps is used for taking pictures of the steam jet condensation. The original images are measured in a size of 64 mm × 128 mm with full resolution of 800 × 1600, so a spatial resolution of 0.08mm/pixel is achieved. The sampling time for each case is 0.1s and shooting frequency of 5000 frames per second. Two phase interface is oscillating with small amplitude due to instabilities, so 500 frame images are averaged to obtain reliable results in each experimental case. This average method is also used by Xu et al. [30] and Weiland and Vlachos [31]. The processing of images consist of conversion, filtering, segmentation and edge detection, as suggested by Xu and Guo [8]. Measurements of steam plume size are carried out by MATLAB software.

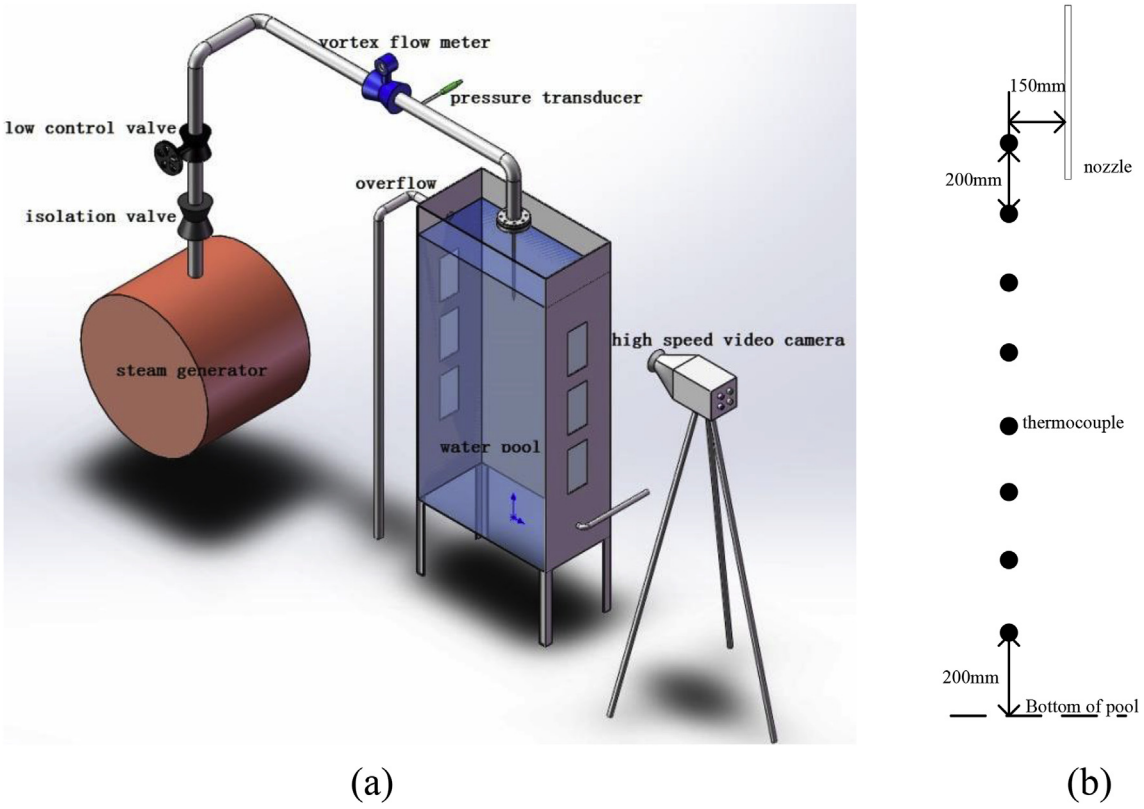

Fig. 2. Schematic diagram of experimental system and thermocouples distribution in water pool (a) experimental system (b) thermocouples distribution in water pool.

Table 1
Experimental conditions.

Parameters	Value
Steam mass velocity G, kg/m^{2}s	320–1080
Water temperature T_w, °C	25–60
Ambient pressure p_a, kPa	103
Diameter of tube nozzle d, mm	10
Submerged depth of nozzle H_{sub}, mm	300
Water depth H, mm	1800
Jet direction	Vertical downward

3. Experimental results and discussion

3.1. Thermal stratification

The suppression pool surface temperature, which determines the vapor partial pressure in the wet well, is very important to overall containment performance. Therefore, the thermal stratification of the SP is of primary importance [32]. As Song [18] pointed out Richardson number representing the ratio of the buoyancy to inertial force in thermal convection can be a criterion for determining whether or not thermal stratification occurred in chugging condensation regime.

$$Ri = \left(\frac{\rho_a - \rho_{sat}}{\rho_{sat}}\right) \frac{g(H - H_{sub})}{u_j^2} \tag{1}$$

where g is the gravitation acceleration, $H - H_{sub}$ is the distance between nozzle tip and pool bottom, u is velocity. In the subscript, *sat* refers to saturated water, j refers to single water jet and a refers to ambient water.

However, for sonic steam jet, u_j can't be calculated by synthetic jet theory. As suggested by Gamble [32], With the assumption of a constant single water jet diameter, conservation of momentum yields an equation for the average velocity of the water jet.

$$u_j = u_e \sqrt{\frac{\rho_s}{\rho_{sat}}} \tag{2}$$

In the subscript, e refers to exit of nozzle and s mean steam. So, for sonic steam jet condensation,

$$Ri = \frac{(\rho_a - \rho_{sat})gl}{u_e^2 \rho_s} = \frac{(\rho_a - \rho_{sat})\rho_s gl}{G_e^2} \tag{3}$$

where u_s is steam velocity of nozzle exit, which is equal to local speed of sound.

Ri is obtained based on Eq. (3) and its values are in the ranges of 0.16–2.67. As the steam mass velocity and water temperature increase, Ri decreases as shown in Fig. 3(a). That is, the injection steam mixes stronger the water in the pool with the increase in steam mass velocity and water temperature, which appeals to common sense. From the water temperature distribution in different heights under the condition of a certain constant steam mass velocity, thermal stratification is not clear as shown in Fig. 3(b). We can conclude that if *Ri* is lower than 2.67, there is no thermal stratification for sonic jet. In the Song's experiment result [18], if *Ri* is lower than 0.1, water pool would be difficult to get stratification in Chugging regime.

3.2. Steam plume shape and condensation regime map

The shape of the steam plume is a significant characteristic on studying steam jet in subcooled water. In the present experiment,

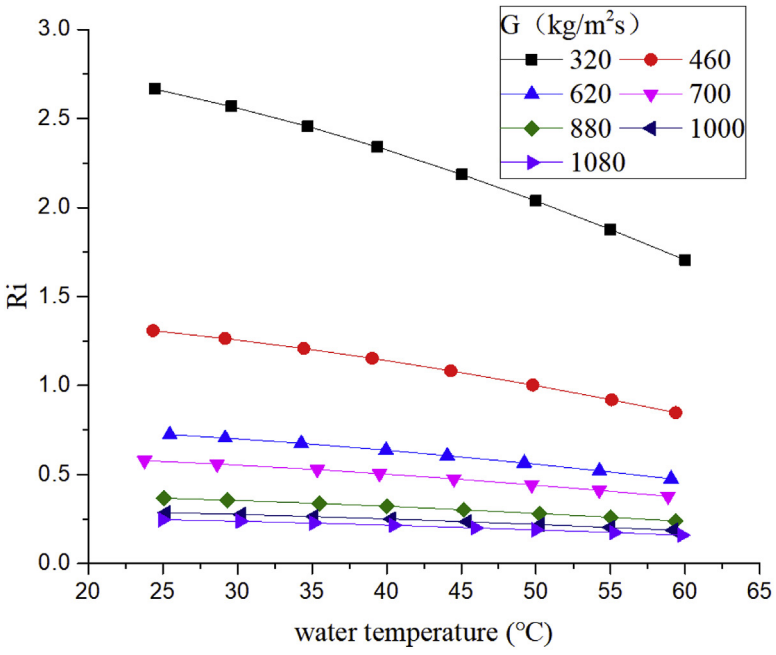

(a)

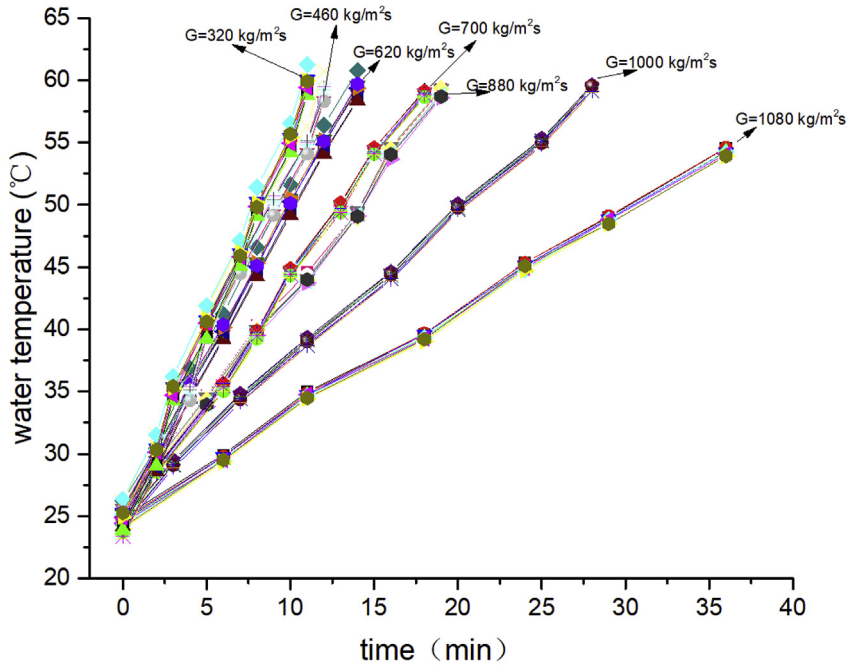

(b)

Fig. 3. (a) Richardson number (b) water distribution in vertical direction.

three typical steam plume shapes and condensation oscillatory regime are observed as shown in Fig. 4 & Fig. 5. Fig. 4(a) shows periodic change of steam plume shape with time in condensation oscillation regime, including three different sequences of events: (i) bubble growth, (ii) bubble translation and (iii) bubble collapse. The sequences of the events are as follows: (1) an oscillation cycle begins with the bubble formation at the pipe outlet. With the increase of the diameter of the bubble, the condensation rate increases and the bubble growth rate is slowed down until the bubble diameter reach maximum. (2) Spherical bubble is elongated by jet momentum force and translates to downstream in vertical direction until jet momentum force weak. (3) The rate of steam flow

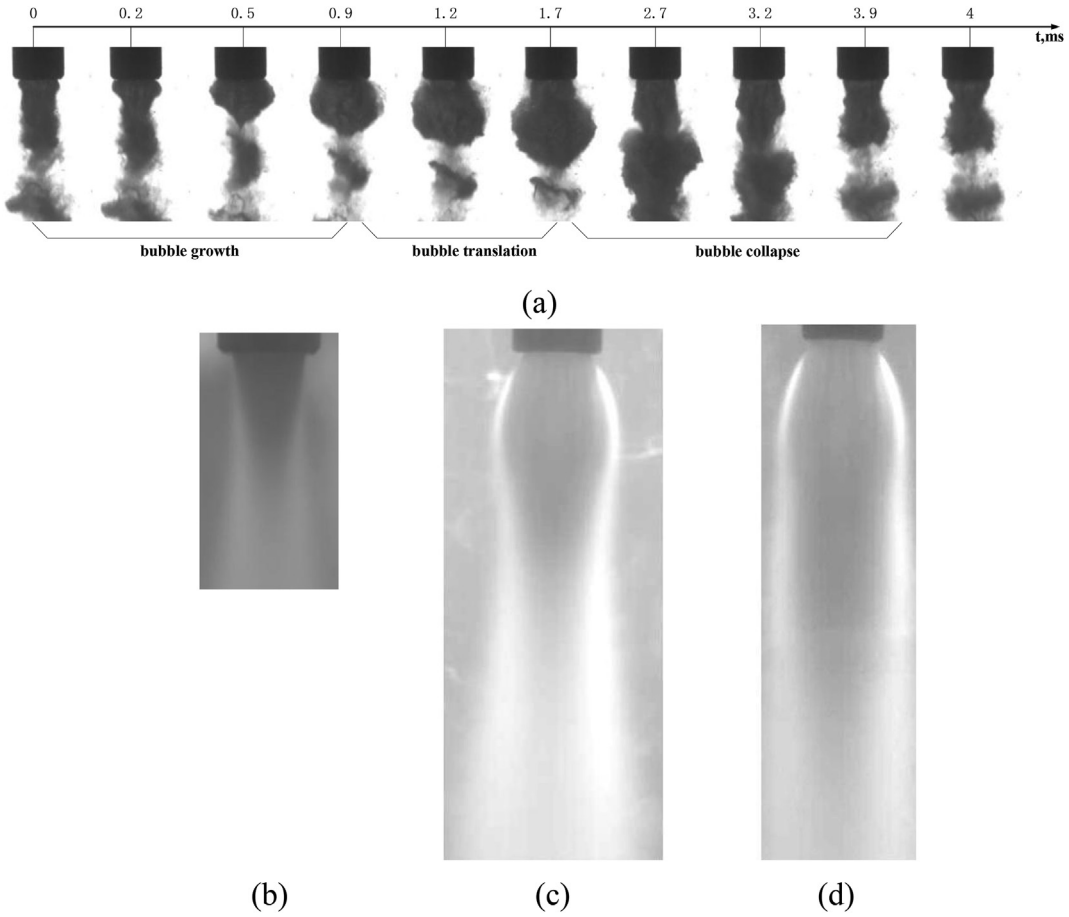

Fig. 4. Four typical steam plume shapes (a) condensation oscillation (b) contraction(c) expansion-contraction (d) double expansion-contraction.

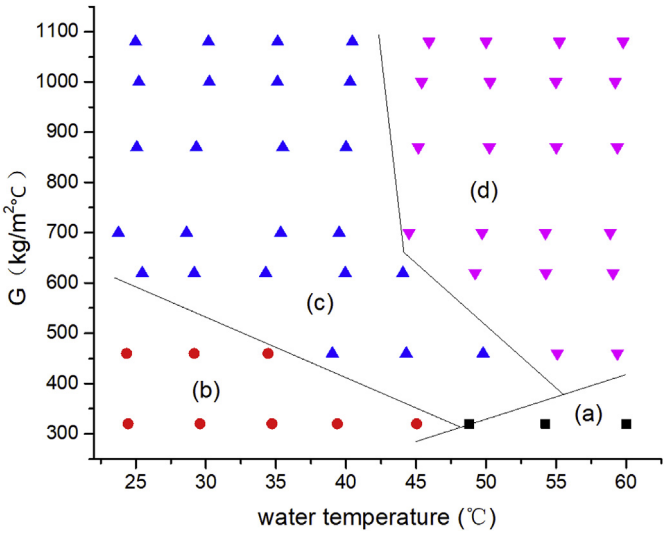

Fig. 5. Condensation regime map.

entering into bubble suddenly decreases, then bubble begins to collapse. Steam bubble appears and disappears periodically with a frequency of about 250 Hz and the oscillation frequency decreases as the water temperature increase. The same phenomenon is also observed by Simpson et al. [33]. Fig. 4(b)-(d) show typical contraction shapes, expansion-contraction shapes and double expansion-contraction shapes of plume shapes in different steam mass velocity and water temperature.

Fig. 5 shows a new condensation regimes map based on steam mass velocity and water temperature in present experimental conditions. Condensation oscillation (a) is observed at low steam mass velocity and high water temperature conditions. Condensation was found to reduce instability of steam-water interface by theoretical analysis of Chan et al. [34]. So, with the reduce of water temperature, the condensation rate is increased. As a result, stability of steam-water interface is strengthened and condensation regime transits to stable regime from unstable regime. Contraction shapes (b) were observed at low steam mass velocity and low water temperature conditions. Low steam mass velocity means under-expansion of steam is low, so the effect of expansion wave and compressive wave is not obvious. Expansion-contraction shapes(c) were observed at high steam mass velocity and low water temperature conditions. High steam mass velocity means under-expansion of steam is high, so the effect of expansion wave and compressive wave is obvious only in the first cell due to the high condensing capacity of subcooled water. Double expansion-contraction shapes (d) were observed at high steam mass velocity and high water temperature conditions. The effect of expansion wave and compressive wave is obvious in the first two cells due to the low condensing capacity of subcooled water.

3.3. Dimensionless steam plume length

Length of steam plume is one of the key parameters for design

for pressure suppression system, which is defined as the minimum distance of steam condensation completely. Dimensionless steam plume length defined as the ratio of steam plume length to nozzle inner diameters obtained by the image processing. The images got from the high-speed camera, according to N. Otsu [35], have an uncertainty coming from the direct measurements, which is also the uncertainty of the steam plume length. We assume that the LED lamp is light enough, so the uncertainty is insignificant.

The results show that dimensionless steam plume length increases gradually with the increase of steam mass velocity and water temperature, which is similar to the previous experimental results, as shown in Fig. 6. With the increase of water temperature, condensing capacity of subcooled water reduces, so under the condition of constant steam flow rate, the gas-liquid interfacial area increases. As a result, dimensionless steam plume length increases.

A new correlation of dimensionless steam plume length was obtained based on the basic form presented by Kerney et al. [27], as shown in Eq. (4).

$$L = 0.1776B^{-1.0327}\left(\frac{G}{G_m}\right)^{-09594.} \tag{4}$$

where $B = c_{p,w}\Delta T/(h_s - h_w)$ is the condensation driving potential, $c_{p,w}$ is water special heat, $\Delta T = T_{sat} - T_w$ is subcooling temperature of water, T_{sat} is saturated water temperature in the ambient pressure, h_s and h_w are the enthalpy of steam and water, respectly. G is steam mass velocity of nozzle exit, G_m is equal to 275 kg/m^{2}s.

Fig. 7 shows the comparison of dimensionless steam plume length between predicted results by Eq. (4) and experimental results got by measuring photos recorded by high-speed camera or from other authors. The discrepancy is in a range from −10% to 10% under present experimental results, and from −25% to 25% for the experimental results of Kerney et al. [27] and Chong et al. [24]. The good consistency between the experimental results and predicted results illustrates Eq. (4) is accurate enough for the condition that the steam mass velocity ranges from 320 to 1080 kg/m^{2}s and the water temperature ranges from 25 to 60 °C.

3.4. Condensation heat transfer coefficient

The average condensation heat transfer coefficient can be calculated based on the thermal balance and Newton cooling equation, as shown in Eq. (5).

$$h = \frac{GA_e(h_s - h_w)}{\Delta TA_i} \tag{5}$$

where A_e is cross-sectional area of nozzle, and A_i is heat transfer area.

Fig. 8 shows the analytical model of steam plume area. Assuming that all the condensation occurs on the boundary of the smooth plume and the plume has a perfect axisymmetric structure, heat transfer area could be calculated by Eq. (6).

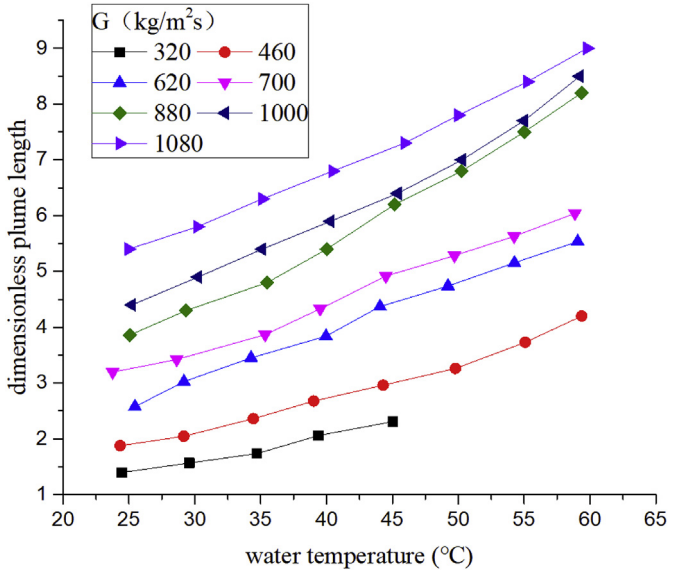

Fig. 6. Dimensionless plume length at various conditions.

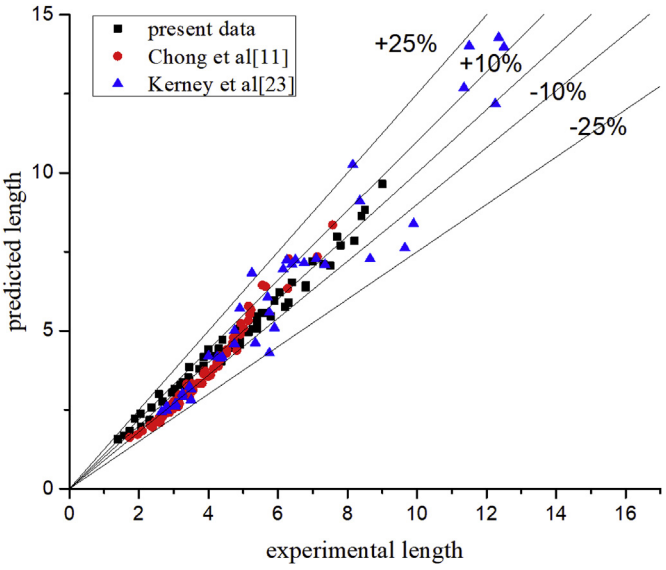

Fig. 7. Comparison of predicted steam plume length with experimental results.

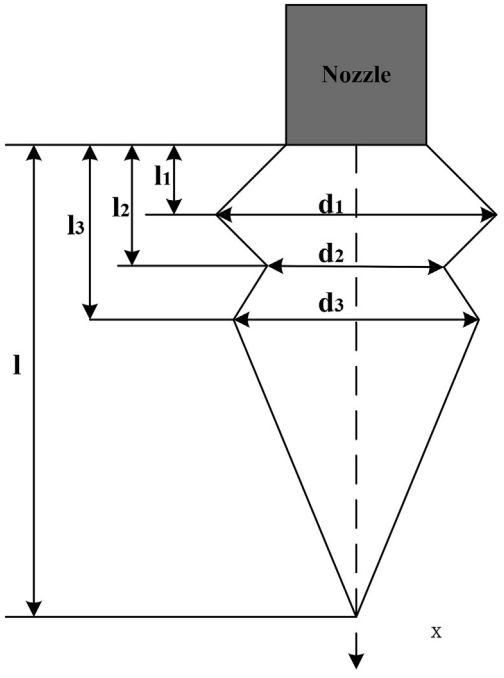

Fig. 8. Analysis model of steam plume area for stable jet condensation.

$$A_i = \int_0^{l_1} \pi\left(d + \frac{x}{l_1}(d_1 - d)\right)dx + \int_{l_1}^{l_2} \pi\left(d_1 + \frac{x - l_1}{l_2 - l_1}(d_2 - d_1)\right)dx + \int_{l_2}^{l_3} \pi\left(d_2 + \frac{x - l_2}{l_3 - l_2}(d_3 - d_2)\right)dx + \int_{l_3}^{l} \pi\left(d_3 + \frac{x - l_3}{l - l_3}(0 - d_3)\right)dx \quad (6)$$

where d, d_1, d_2 and d_3 are nozzle diameter, the first expansion diameter, the first contracted diameter and the second expansion diameter, respectly. l, l_1, l_2 and l_3 are plume length, axial distance of the first expansion diameter, the first contracted diameter and the second expansion diameter, respectly. For contraction shapes regime, $d_1 = d_2 = d_3 = 0$, $l_1 = l_2 = l_3 = 0$. For expansion-contraction shapes regime, $d_2 = d_3$, $l_2 = l_3$.

Fig. 9 shows results of condensation heat transfer coefficient and its values are in the range of 1.44–3.65 MW/m^2·K in present experimental condition. As the water temperature increases, condensation heat transfer coefficient decreases gradually which is also found by previous researchers. As the steam mass velocity increases, condensation heat transfer coefficients increase in contraction shapes regime, but the opposite trend in expansion-contraction shapes and double expansion-contraction shapes regime. The similar trend is observed by Wu et al. [16]. In expansion-contraction shapes and double expansion-contraction shapes regime, the condensation process is mainly controlled by the effect of expansion wave and compressive wave. The diameter of steam plume increases with the increases of steam mass velocity. As a result, condensation heat transfer coefficients decreases due to the increase of heat transfer area.

A new correlation of condensation heat transfer coefficients is obtained based on condensation driving potential and dimensionless steam mass velocity, as shown in Eq. (7).

$$h = 7.125\, B^{0.354}\left(\frac{G}{G_m}\right)^{-0.551} \quad (7)$$

Fig. 10 shows the comparison of condensation heat transfer coefficients between predicted result by Eq. (7) and experimental result. The discrepancy is in a range from −12% to 12% in the most

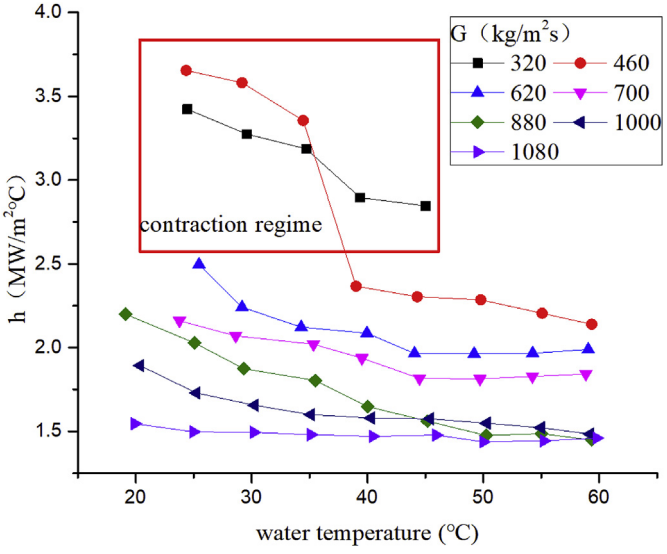

Fig. 9. Condensation heat transfer coefficients at various conditions.

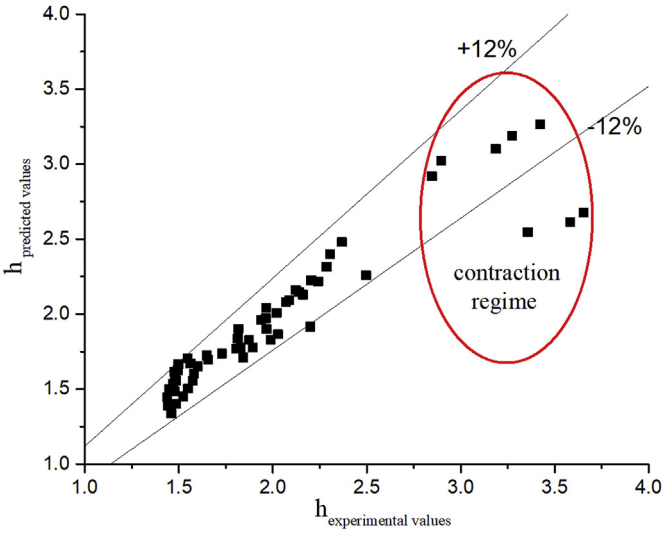

Fig. 10. Comparison of predicted results with experimental results.

experimental condition. Condensation heat transfer coefficient is underestimated 20% by Eq. (7) in higher steam mass velocity for contraction shape regime.

The uncertainty of equation (7) is analyzed as follow.

$$h = 7.125\left(\frac{c_{p,w}\Delta T}{h_s - h_w}\right)^{0.354}\left(\frac{G}{G_m}\right)^{-0.551} = C{*}G^{-0.551}{*}\left\{\frac{(T_{sat} - T_w)}{(h_s - h_w)}\right\}^{0.354} \quad (8)$$

while $C = \frac{7.125 c_{p,w}^{0.354}}{G_m^{-0.551}}$, which was considered as constant.

Obviously,

$$dh = d\left(C{*}G^{-0.551}{*}\frac{(T_{sat} - T_w)^{0.354}}{(h_s - h_w)}\right) = -0.551\frac{h}{G}dG + 0.354\frac{h}{T_{sat} - T_w}d(T_{sat} - T_w) - 0.354\frac{h}{h_s - h_w}d(h_s - h_w) \quad (9)$$

As a result,

$$\frac{dh}{h} = -0.551\frac{dG}{G} + 0.354\frac{d(T_{sat} - T_w)}{T_{sat} - T_w} - 0.354\frac{d(h_s - h_w)}{h_s - h_w} \quad (10)$$

The max of related tolerances are

$$\frac{dG}{G} = 0.012 \quad (11)$$

$$\frac{d(T_{sat} - T_w)}{T_{sat} - T_w} = 0.015 \quad (12)$$

$$\frac{d(h_s - h_w)}{h_s - h_w} \le \frac{dP}{P} + \frac{dT}{T} = 0.110 + 0.015 = 0.125 \quad (13)$$

So the $\frac{dh}{h} \le 0.152$, which meets the consequence got by experimental data.

4. Conclusions

Series of experiment were conducted to study sonic steam jet

condensation submerged in quiescent subcooled water. Thermal stratification, condensation regime, steam plume length and condensation heat transfer coefficient are discussed under the conditions of different water temperature and steam mass velocity. Conclusions could be drawn as follows:

(1) Richardson number was in the range of 0.16–2.67 in present experiment and there was no thermal stratification observed for sonic steam jet condensation.
(2) Four condensation regimes were observed, including condensation oscillation, contraction, expansion-contraction and double expansion-contraction shapes. A condensation regime map was present based on experimental observation.
(3) Dimensionless steam plume length was obtained by image processing, and increases with the increase of steam mass velocity and water temperature. A new correlation of dimensionless steam plume length was developed and the discrepancy was in a range from −10% to 10% under present experimental results and from −25% to 25% for the previous experimental results.
(4) Condensation heat transfer coefficients were in range of 1.44–3.65 MW/m^2°C under present experimental conditions. As the increase of water temperature, condensation heat transfer coefficients decreased gradually. As the steam mass velocity increases, condensation heat transfer coefficients increase in contraction shapes regime, but the opposite trend in expansion-contraction shapes and double expansion-contraction shapes regime. A new correlation of condensation heat transfer coefficients was developed and the discrepancy was in a range from −12% to 12% for most experimental results.

Acknowledgement

The financial supports of National Nature Science Foundation of China (Nos. 11605032, 11605033) and the Fundamental Research Funds for the Central Universities of Ministry of Education of China (Grant No. GK2150260157) are gratefully acknowledged.

Appendix A. Supplementary data

Supplementary data to this article can be found online at https://doi.org/10.1016/j.net.2019.02.003.

Nomenclature

Notation

A	area, m^2
B	condensation driving potential
C	constant
d	nozzle diameter, mm
D	dimensionless diameter
G	steam mass velocity, kg/m^2 s
h_s	specific enthalpy of steam, J/kg
h_w	specific enthalpy of water, J/kg
H	condensation heat transfer coefficient, W/m^{2}s
H	depth, mm
L	steam plume length, m
L	dimensionless steam plume length
R	radius, m
T	temperature, °C
ΔT	Subcooling degree, °C
T	time, s
ρ	density, kg/m^3

Subscripts

A	ambient
E	exit of pipe
I	interface of steam and water
Sat	saturation
Max	maximum
S	steam
W	water
Sub	submerge

References

[1] B.G. Jeon, H.C. No, Conceptual design of passive containment cooling system with air holdup tanks in the concrete containment of improved APR+, Nucl. Eng. Des. 267 (2014) 180–188.
[2] Vladimir N. Blinkov, O.I.M., Vladimir I. Melikhov, Mikhail V. Davydov, S.A. HolgerWolff, Experimental Studies for the VVER-440/213 Bubble Condenser System forKolaNPP at the Integral Test Facility BCV-213, 2011.
[3] C.K. Chan, C.K.B. Lee, A regime map for direct contact condensation, Int. J. Multiph. Flow 8 (1) (1982) 11–20.
[4] M.H. Chun, Y.S. Kim, J.W. Park, An investigation of direct condensation of steam jet in subcooled water, Int. Commun. Heat Mass Transf. 23 (7) (1996) 947–958.
[5] S. Cho, C.H. Song, C.K. Park, S.K. Yang, M.K. Chung, Experimental study on dynamic pressure pulse in direct contact condation of steam jets discharging into subcooled water, in: Proceedings of NTHAS98, 1998.
[6] A. Petrovic de With, R.K. Calay, G. de With, Three-dimensional condensation regime diagram for direct contact condensation of steam injected into water, Int. J. Heat Mass Transf. 50 (9–10) (2007) 1762–1770.
[7] X.-Z. Wu, et al., Condensation regime diagram for supersonic/sonic steam jet in subcooled water, Nucl. Eng. Des. 239 (12) (2009) 3142–3150.
[8] Q. Xu, L. Guo, Direct contact condensation of steam jet in crossflow of water in a vertical pipe. Experimental investigation on condensation regime diagram and jet penetration length, Int. J. Heat Mass Transf. 94 (2016) 528–538.
[9] Q. Xu, et al., Condensation regime diagram for supersonic and subsonic steam jet condensation in water flow in a vertical pipe, Appl. Therm. Eng. 130 (2018) 62–73.
[10] W. Chen, et al., Characteristic of pressure oscillation caused by turbulent vortexes and affected region of pressure oscillation, Exp. Therm. Fluid Sci. 76 (2016) 24–33.
[11] S.J. Hong, et al., Condensation dynamics of submerged steam jet in subcooled water, Int. J. Multiph. Flow 39 (2012) 66–77.
[12] D. Chong, et al., Experimental and theoretical study on the second dominant frequency in submerged steam jet condensation, Exp. Therm. Fluid Sci. 68 (2015) 744–758.
[13] B. Qiu, et al., Experimental investigation on the second dominant frequency of pressure oscillation for sonic steam jet in subcooled water, Exp. Therm. Fluid Sci. 58 (2014) 131–138.
[14] S. Fukuda, Pressure variation due to vapor condensation in liquid (II): phenomena at large vapor mass flow rate, J. Atom. Energy Soc. (1982) 466–474.
[15] F. Yuan, et al., Pressure oscillation of submerged steam condensation in condensation oscillation regime, Int. J. Heat Mass Transf. 98 (2016) 193–203.
[16] X.-Z. Wu, et al., Experimental study on sonic steam jet condensation in quiescent subcooled water, Chem. Eng. Sci. 64 (23) (2009) 5002–5012.
[17] X.-p. Yang, et al., Experimental study on the direct contact condensation of the steam jet in subcooled water flow in a rectangular channel: flow patterns and flow field, Int. J. Heat Fluid Flow 56 (2015) 172–181.
[18] D. Song, et al., Dimensional analysis of thermal stratification in a suppression pool, Int. J. Multiph. Flow 66 (2014) 92–100.
[19] H. LI, Effective models for simulation of thermal stratification and mixing induced by steam injection into a large pool of water, in: KUNGLIGA TEKNISKA HÖGSKOLAN, 2014.
[20] D. Song, et al., Relationship between thermal stratification and flow patterns in steam-quenching suppression pool, Int. J. Heat Fluid Flow 56 (2015) 209–217.
[21] Y.J. Choo, C.H. Song, PIV measurements of turbulent jet and pool mixing produced by a steam jet discharge in a subcooled water pool, Nucl. Eng. Des. 240 (9) (2010) 2215–2224.
[22] H.J. Hussein, S.P. Capp, W.K. George, Velocity measurements in a high-Reynolds-number, momentum-conserving, axisymmetric, turbulent jet, J. Fluid Mech. 258 (1994) 31–75.
[23] X.-Z. Wu, et al., Experimental study on the condensation of supersonic steam jet submerged in quiescent subcooled water: steam plume shape and heat transfer, Int. J. Multiph. Flow 33 (12) (2007) 1296–1307.
[24] D. Chong, et al., Research on the steam jet length with different nozzle structures, Exp. Therm. Fluid Sci. 64 (2015) 134–141.
[25] H.Y. Kim, et al., Experimental study on stable steam condensation in a quenching tank, Int. J. Energy Res. 25 (2001) 239–252.
[26] J.C. Weimer, G.M. Faeth, D.R. Olson, Penetration of vapor jets submerged in subcooled liquids, AIChE J. 19 (3) (1973) 552–558.
[27] P.J. Kerney, G.M. Faeth, D.R. Olson, Penetration characteristics of a submerged

steam jet, AIChE J. 18 (3) (1972) 548–553.
[28] Y.S. Kim, J.W. Park, C.-H. Song, Investigation of the stem-water direct contact condensation heat transfer coefficients using interfacial transport models, Int. Commun. Heat Mass Transf. 31 (3) (2004) 397–408.
[29] A. Khan, et al., Experimental investigations of the interface between steam and water two phase flows, Int. J. Heat Mass Transf. 73 (2014) 521–532.
[30] Q. Xu, L. Guo, L. Chang, Interfacial characteristics of steam jet condensation in crossflow of water in a vertical pipe, Appl. Therm. Eng. 113 (2017) 1266–1276.
[31] C. Weiland, P.P. Vlachos, Round gas jets submerged in water, Int. J. Multiph. Flow 48 (2013) 46–57.
[32] R.E. Gamble, et al., Pressure suppression pool mixing in passive advanced BWR plants, Nucl. Eng. Des. 204 (1–3) (2001) 321–336.
[33] M.E. Simpson, C.K. Chan, Hydrodynamics of a subsonic vapor jet in subcooled liquid, J. Heat Tran. 104 (271) (1982).
[34] S.H. Chan, Y.S. Wang, C.C. Tan, The effect of mass transfer on Kelvin-Helmholtz instability at the gas-liquid interface of a sonic reacting and non-reacting gas jet submerged in a liquid, Int. J. Heat Mass Transf. 37 (7) (1994) 1123–1132.
[35] N. Otsu, A threshold selection method from gray-level histograms, IEEE Trans. Syst. Man Cybern. 9 (1) (1979) 62–66.